International Journal of Nanomedicine

Dovepress
open access to scientific and medical research

Open Access Full Text Article

ORIGINAL RESEARCH

Molecular Antenna-Sensitized Upconversion Nanoparticle for Temperature Monitored Precision Photothermal Therapy

This article was published in the following Dove Press journal:
International Journal of Nanomedicine

Yanchun Wei
Sen Liu
Changjiang Pan
Zhongmei Yang
Ying Liu
Jianfang Yong
Li Quan

Jiangsu Provincial Engineering Research Center for Biomedical Materials and Advanced Medical Devices, Huaiyin Institute of Technology, Huai'an, Jiangsu, People's Republic of China

Background: Photothermal therapy with accurate and real-time temperature detection is desired in clinic. Upconversion nanocrystals (UCNs) are candidate materials for simultaneous temperature detection and photothermal agents carrying. However, the weak luminescence and multiple laser excitations of UCNs limit their application in thermal therapy.

Materials and Methods: $NaYF_4$:Yb^{3+},Er^{3+},Nd^{3+}, PL-PEG-NH_2, IR-806 and folic acid are selected as structural components. A nanoprobe (NP) integrated with efficient photothermal conversion and sensitive temperature detection capabilities is synthesized for precise photothermal therapy. The probes are based on near-infrared upconversion nanocrystals doped with Yb, Er and Nd ions, which can be excited by 808 nm light. IR-806 dye molecules are modified on the surface as molecular antennas to strongly absorb near-infrared photons for energy transfer and conversion.

Results: The results show that under an 808 nm laser irradiation upconversion luminescence of the nanocrystals is enhanced based on both the Nd ion absorption and the FRET energy transfer of IR-806. The luminescence ratio at 520 and 545 nm is calculated to accurately monitor the temperature of the nanoparticles. The temperature of the nanoprobes increases significantly through energy conversion of the molecular antennas. The nanoparticles are found successfully distributed to tumor cells and tumor tissue due to the modification of the biocompatible molecules on the surface. Tumor cells can be killed efficiently based on the photothermal effect of the NPs. Under the laser irradiation, temperature at mouse tumor site increases significantly, tissue necrosis and tumor cell death can be observed.

Conclusion: Precision photothermal therapy can thus be achieved by highly efficient near-infrared light absorption and accurate temperature monitoring, making it promising for tumor treatment, as well as the biological microzone temperature detection.

Keywords: temperature, photothermal therapy, molecule antennas, upconversion nanoparticle

Introduction

Numerous methods have been developed for cancer treatment. Significant efforts have been reported, although each of these methods has its own limitations. Among them, thermal therapy is an important treatment modality among them. Many thermal sources are used for this method, such as microwave, radiofrequency and near-infrared light.[1–3] As a local therapeutic modality, photothermal therapy (PTT) utilizes photoabsorbers to generate heat from near-infrared light absorption, leading to the thermal ablation of cancer cells.[4] During PTT, chromophores contained in healthy tissue within the light path can also absorb energy, reducing the effectiveness of heat

Correspondence: Yanchun Wei; Li Quan
Jiangsu Provincial Engineering Research Center for Biomedical Materials and Advanced Medical Devices, Huaiyin Institute of Technology, Huai'an, Jiangsu, People's Republic of China
Tel +86-137 1691 3791
Email weiyanchunha@hyit.edu.cn; quanli2016@hyit.edu.cn

submit your manuscript | www.dovepress.com
DovePress
http://doi.org/10.2147/IJN.S236371

deposition within tumor cells and increasing nonspecific injury to adjacent healthy tissue. Therefore, in situ light-absorbing agents are often used to selectively increase the thermal destruction of the targeted tumors and to reduce injury to normal tissues.[5–8]

PTT uses high temperature to damage tumor cells by heating the lesions.[9–11] During treatment, the temperature can range from 40°C to more than 50°C, comparing hyperthermia (40–41°C),[12] moderate-temperature hyperthermia (42–45°C),[13] and thermal ablation, or high-temperature hyperthermia (>50°C).[14] The current method used to monitor PTT regards the entire lesion containing PTT agents as a macroscopic heat source and keeps the overall temperature of the lesion at a high level in line with the temperature definition for conventional thermal therapy. Such a high apparent temperature can damage normal tissues adjacent to the lesions due to massive heat transfer, thereby, leading to increased side effects and inhibiting the therapeutic accuracy of PTT. Therefore, accurate temperature monitoring is required.

Temperature can be measured via a diverse array of sensors. All of them infer temperature by sensing some change in a physical characteristic. During PTT, there are normally three methods for temperature measurement: using a thermal sensor, detecting infrared light emitted by tissues and monitoring the properties of a thermal absorber. Using additional thermal sensors is invasive and size limited. Infrared thermometry is limited by the light penetration suitable for surface temperature detection. Measuring temperature by using multifunctional nanoparticles integrated with a temperature probe and a thermal absorber has advantages during PTT due to the precise localization of the temperature probe. In recent decades, these thermometric techniques, especially optical temperature-sensing probes have been rapidly developed and are a promising platform for precise PTT.

Optical temperature probes mainly include organic dyes, polymers, quantum dots and lanthanide-based upconversion nanocrystals (UCNs).[13,15-18] Among them, UCNs allow the conversion of lower-energy light in the near-infrared region into higher energy emissions. During the energy conversion process, the electronic transition probabilities at different energy levels are differently influenced by temperature.[19] Moreover, when used in biomedicine, UCNs show many advantages such as their superior photostability, nonblinking property, absence of autofluorescence of biological tissue and use of low-energy NIR radiation.[20,21] On the basis of the above merits, UCNs are ideal probes for real-time sensing of the eigen temperature of PTT agents in biological systems.

UCNs can be excited mainly by light at two near-infrared wavelengths, 808 nm or 980 nm absorbed by Nd^{3+} and Yb^{3+} respectively.[22,23] For PTT use, 808 nm UCNs are preferred over 980 nm UCNs due to the lower water absorption and deeper tissue penetration of light at the former wavelength.[24,25] However, UCNs are not a good agent for direct use in PTT due to their limited absorption of light. Although UCNs can absorb near-infrared light and emit visual light under irradiation, their absorption is still low for PTT. The limited energy transformation of UCNs cannot effectively increase the temperature. In addition, the luminescence efficiency of UCNs excited by 808 nm light is lower than that of UCNs excited by 980 light, thus limiting their sensitivity for temperature monitoring. Therefore, modifications of UCNs using high light-absorbing agents as molecular antennas to transform energy for increasing the temperature rising[13,26] or for realizing highly efficient luminescence have been studied.[27,28]

An optical temperature-sensing technique using UCNs as a PTT thermometer based on the fluorescence intensity ratio of green upconversion emission by the Er^{3+} doped and Er^{3+}–Yb^{3+} codoped materials has attracted much attention, because it can reduce the dependence on measurement conditions and improve the sensitivity by measuring the fluorescence intensity originating from the $2H_{11/2} \rightarrow 4I_{15/2}$ and $4S_{3/2} \rightarrow 4I_{15/2}$ transitions of Er^{3+}. The ratio of which is independent of fluorescence loss and fluctuations in excitation intensity.[13,29] Here we built a near-infrared absorber-coated upconversion nanocomposite $NaYF_4$:Yb,Er,Nd@IR-806/PL-PEG-FA, to enhance the sensitivity for temperature sensing and improve the therapeutic effect of PTT. The multifunctional nanoparticles can be simultaneously used for PTT and temperature monitoring by only absorbing an 808 nm laser, which is a light with deep penetration in biological tissue. The high sensitivity and precise temperature response make these nanoparticles a good agent for enhanced PTT.

Materials and Methods

Materials

The Rare-earth acetates $(CH_3COO)_3Y{\cdot}4H_2O$, $(CH_3COO)_3Yb{\cdot}4H_2O$, $(CH_3COO)_3Nd{\cdot}4H_2O$ and $(CH_3COO)_3Er{\cdot}4H_2O$; 1-ethyl-3-(3-dimethylaminopropyl) carbodiimide hydrochloride (EDC); N-hydroxysuccinimide (NHS); oleic acid; and cyclohexane were purchased from Aladdin Reagent, Ltd.

2-distearoyl-sn-glycero-3-phosphoetha-nolamine-N-[carboxy (polyethyleneglycol)-2000] (PL-PEG-NH_2) was purchased from Avanti Polar Lipid Co., Ltd. Folic acid (FA), IR-780 ($C_{36}H_{44}N_2$) and Hoechst were purchased from Sigma-Aldrich Co., Ltd. All chemicals were of analytical grade. CCK-8 was obtained from Dojindo China Co. Ltd. RPMI 1640 cell culture medium, fetal bovine serum, penicillin, and streptomycin were obtained from Gibco Invitrogen. All aqueous solutions were prepared using ultrapure water, which was obtained through an Advanced-iv-08 water purification system (Chengdu, China).

$NaYF_4$:Yb,Er,Nd Synthesis

$NaYF_4$:Yb,Er and $NaYF_4$:Yb,Er,Nd UCNs were synthesized via a hydrothermal synthesis method. In a typical procedure for the synthesis of $NaYF_4$:10%Yb^{3+},1%Er^{3+},2%Nd^{3+} UCNs, 30 mmol of NaOH was dissolved in 3 mL of DI water. Next, 8 mL of ethanol and 20 mL of Oleic acid were added to the above solution with constant stirring for 20 min. Then, 0.885 mmol of $Y(CH_3COO)_3{\cdot}4H_2O$, 0.1 mmol of $Yb(CH3COO)_3{\cdot}4H_2O$, 0.005 mmol of $Er(CH_3COO)_3{\cdot}4H_2O$ and 0.01 mmol of $Nd(CH_3COO)_3{\cdot}4H_2O$ (with and without) were added and stirred for another 30 min. Subsequently, 10 mL of ethanol containing 10 mmol of NaF was added to the above solution and stirred for another 30 mins. The resulting mixture was then transferred into a 50 mL stainless Teflon-lined hydrothermal reactor, to be sealed and heated to 190°C for 24 hrs. After that, the hydrothermal reactor was cooled to room temperature naturally, and the reaction mixture was separated through centrifugation (6000 rpm, 5 mins). The precipitate was washed with cyclohexane, ethanol and DI-water several times and dried under vacuum at 40°C for 12 hrs to obtain the $NaYF_4$:Yb,Er and $NaYF_4$:Yb,Er,Nd nanoparticles.

Modification of Nanoparticles with IR-806 Dye and Folic Acid

PL-PEG-NH_2 (5 mg) and UCNs (10 mg) were added into 10 mL of DMSO and then dispersed with ultrasound for 30 mins. The mixed solution was stirred for 10 mins and purified by centrifugation at 6000 rpm for 5 mins. The obtained PL-PEG-NH_2-coated UCNs were dispersed in 10 mL of DMSO (repeated two times for purification).

IR-806 was routinely synthesized under a dry N_2 atmosphere.[27] A mixture of IR-780 iodide (500 mg, 0.75 mmol) and 4-mercaptobenzoic acid (231 mg, 1.50 mmol) in DMF (20 mL) was stirred at room temperature. After 17 hrs, DMF was removed under vacuum at 40ºC. The residue was dissolved in CH_2Cl_2 (8 mL) and filtered through a 0.45 μm PTFE syringe filter. Diethyl ether (150 mL) was added slowly to precipitate the product. The precipitate was collected by centrifugation, washed with diethyl ether, and dried under vacuum to obtain the final product.

IR-806 (0.1 mg) and folic acid (0.02 mg) were activated with EDC/NHS (1×10^{-4} mol) in DMSO (10 mL) solution. After 30 mins, the PL-PEG-NH_2 coated UCN solution (containing UCNs 5 mg) was added and stirred at room temperature for 4 hrs. The reaction product was purified by centrifugation at 10,000 rpm for 5 mins and suspended in 5 mL of DMSO (repeated three times for purification). UCNs modified with other mass ratios of IR-806 (1:25 and 1:100) were also obtained.

Characterization of the Nanoprobes (NPs)

The as-prepared NPs (IR-806 and folic acid-modified UCNs) were dispersed in 1 mL of water in a quartzose cuvette. Samples of NPs were prepared by placing a drop of dilute aqueous dispersions on the surface of a copper grid. The sizes and morphologies were determined at 200 kV using a JEOL JEM-2010F high-resolution transmission electron microscope (HR-TEM). Deionized water was used throughout.

Desiccated UCNs and NPs (1 mg) were prepared. Fourier transform infrared (FT-IR) spectra were recorded on a Tersor 27 spectrometer (Bruker, Ettlingen, Germany) at room temperature. To detect the hydrodynamic size and stability of NPs, the NPs were fully diluted with three different aqueous solutions: deionized water, saline and RPMI 1640 solutions, and left to stand 0 or 24 hrs.[30] The hydrodynamic sizes were then detected by a particle size instrument (Zetasizer nano-ZS90, Malvern Instruments Ltd., Malvern, UK).

NPs in water (0.2 mg/mL) were irradiated with an 808 nm laser (0.2 W/cm^2) and the luminescence was recorded with a visible light camera. The luminescence of $NaYF_4$:Yb,Er, Nd@ PL-PEG-FA at the same concentration was used as a control.

Absorption and Emission Spectra Detection

IR-806 was dissolved in water (100 μM) and put into a quartzose cuvette. After that, the emission spectrum from 810 to 1100 nm and the absorption spectrum from 300 to 1000 nm were measured by a fiber spectrometer (QE65000, Ocean Optical Co., Ltd., Dunedin, USA). The

as-prepared NPs (0.2 mg/mL), including those modified with different IR-806 and those doped with different ions, were dispersed in 1 mL of water. The solution was added to a quartzose cuvette and irradiated by an 808 nm laser. The emission spectrum from 810 to 1000 nm and the absorption spectrum from 500 to 1000 nm were measured by the above-mentioned fiber spectrometer.

Upconversion emission spectra of different synthesized upconversion nanoparticles were also detected with the fiber spectrometer, including those modified with different IR-806 mass ratios (IR-806/UCN: 1:25, 1:50 and 1:100), nanoparticles with or without Nd doping and nanoparticles with or without IR-806 capping.

Temperature Detection with the NPs

NPs (0.2 mg/mL) were dispersed in 1 mL of water, and then transferred into a quartzose cuvette, the temperature of which can be controlled by an electronic hot plate (6k-2020, Taiwan, China). During irradiation with an 808 nm laser, the emission spectrum of the NPs from 400 to 750 nm were measured by a fiber spectrometer. Simultaneously, the temperature was detected with a thermal camera (TVS200EX, NEC, Japan) for comparison. In another experiment, the nanoprobe aqueous solution was dispersed in a vessel. An 808 nm laser (0.6 W/cm^2) was used to irradiate the center of the solution. The temperature of the solution was imaged with a thermal camera.

Assessment of Nanoprobe Effects on Cells

Mouse tumor cells (mouse mammary carcinoma EMT-6 cell line purchased from Fourth Military Medical University Experimental Centre, China.) were cultured in RPMI 1640 cell culture medium. By supplemented with 10% fetal bovine serum and 1% penicillin-streptomycin, the cells were incubated at 37°C in a humidified incubator under 5% CO_2. The cell line and cell procedures were approved by the Institutional Animal Care and Use Committee of Nanjing University.

To study the specific cell-targeting ability of the nanoprobes, EMT-6 tumor cells were seeded into 35 mm confocal culture dishes at the concentration of 10^6 cells per culture dish (500 μL of culture medium) and allowed to grow for 24 hrs. After that, the EMT-6 cells were incubated with fresh RPMI-1640 medium mixed with NPs (0.5 mg/mL, 500 μL) for 4 hrs. The culture medium was then washed with PBS to fully remove any excess nanoparticles. Light images of the nanoparticles in green channels (500–550 nm) were acquired using an upconversion luminescence microscope with an external 808 nm laser (0.6 W/cm^2).

Cells were seeded in dishes for experiments as described above. A Hoechst staining assay (Hoechst 33258) was used to confirm the hyperthermic effect of the NPs on cells (Nanoprobe: 0.5 mg/mL, laser: 0.6 W/cm^2). Briefly, the prepared cells were incubated with NPs for 10 hrs, and then washed twice with PBS. After irradiation with an 808 nm laser at room temperature for 500 s, the cells were stained with 200 μL of bis-benzimide (5 μg/mL) for another 10 mins. Then, the cells were examined using a fluorescence microscope (Axio image A2, Carl Zeiss Inc., Hallbergmoos, Germany) to determine nucleus fragmentation and chromatin condensation.

EMT-6 cells were collected and then seeded into 96-well plates (10^4 cells per well). After the cells were cultured for 24 hrs at 37°C in a humidified incubator, NP PBS solutions (50 μL) were added to the wells. Afterward, the cells were incubated for another 4 hrs at 37°C. Then, the EMT-6 cells were washed using PBS buffer to remove the unbound nanoparticles and excited under an 808 nm laser. During this process, the irradiation time and concentration were used as the variables for testing two cell groups (0–640 s, 0.5 mg/mL, 0.6 W/cm^2 and 0.025–3.2 mg/mL, 0.6 W/cm^2, 500 s). After incubation at 37°C for another 12 hrs, 500 μL of 10% CCK-8 1640 solution was added into each well. Two hours later, the absorbance value at 450 nm was measured with a 96-well plate reader (Flx800, Bio-Tek instrument Inc., Thermo, Germany) to determine the cell viability. The cell viability was calculated as follows: cell viability (% of control) = ODTre/ODCon × 100% (where ODTre is the absorbance value of treated cells and ODCon is the absorbance value of untreated cells). Four samples were used for each study.

Assessment of Nanoprobe Effects for Mouse

Balb/c nude mice (5 weeks old) were obtained from the Laboratory Animal Center of Nanjing Medical University (Nanjing, China). The animal procedures were in accordance with the guidelines of the Institutional Animal Care and Use Committee of Nanjing University. EMT-6 cells (1×10^7 cells/mL, 100 μL) were inoculated subcutaneously into the back of a nude mouse. Once the volume approached 100 mm^3, the mouse was anaesthetized with pentobarbital sodium (i.p., 60 mg/kg) and intravenously injected with 100 μL of the NPs (10 mg/mL). Twelve hours later, the mouse was treated with

an 808 nm laser in situ (0.8 W/cm^2) for 10 mins. During the treatment, temperature at the tumor was recorded with a thermal imager and the luminescence of NPs was detected with a cooled visible light CCD (Sony ICX694, Japan) through a 500–550 nm bandpass filter. At 6 hrs after the thermal therapy, the treated mouse was imaged with the CCD camera, and then the tumor tissues and organs of the mouse were excised, fixed in 10% paraformaldehyde solution and subsequently processed routinely into paraffin. The mouse for control was treated as above but no injection and irradiation. All the sliced tissues were stained with H&E and examined by a Zeiss fluorescence microscope system.

Results and Discussion

The fabrication process and performance mechanism of the NPs are shown in Figure 1. Oil acid-coated UCNs were first loaded with PL-PEG-NH_2. IR-806 and folic acid were then modified onto the surface of UCNs by a hydrophobic reaction to enhance their water solubility, biological compatibility and cell-targeting capability (Figure 1A). The structures of the molecules used are shown in Figure S1. When excited with an 808 nm laser, the upconversion NPs can emit 520 and 545 nm visible light through the dual excitation, a FRET (fluorescence resonance energy transfer) and a direct process. In the FRET process, energy transfers to IR-806 first and then transfers to Yb ions by FRET. In the direct excitation process, energy is absorbed by Nd ions directly and then transferred to Yb ions. All the energy input would be upconverted by the nanocrystal to emit light. The temperature of the NPs increases simultaneously due to the strong light energy absorption of the fluorochrome IR-806. The heating effect is proposed to be used for thermal therapy (Figure 1B).

The luminescence efficiency of the UCNs was optimized through the change of the content of Er ions, and the proportion of Er^{3+} at 1% was selected (Figure S2). The TEM images (in Figure 2A and B) show that the UCNs are hexagonal crystals, with sizes of approximately 50 nm (Figure 2C). When the nanoprobes modified by IR-806 and PL-PEG were dispersed in water, saline and RPMI 1640 separately, each solution showed a good suspension stability, but the average hydrodynamic sizes were all observed increased, approximate 65 nm in water and saline, and 82 nm in cell culture medium (Figure 2D). The distinctive expansion in the culture medium is deduced due to the serum protein absorption. Research has shown that nanoparticle size is an important factor for their in vivo distribution and clearance.[31] The results suggested that the size of NPs was suitable for their in vivo application. FT-IR (Fourier Transform Infrared Spectroscopy) spectra of oleylamine-coated UCNs and IR-806/PL-PEG-coated UCNs are

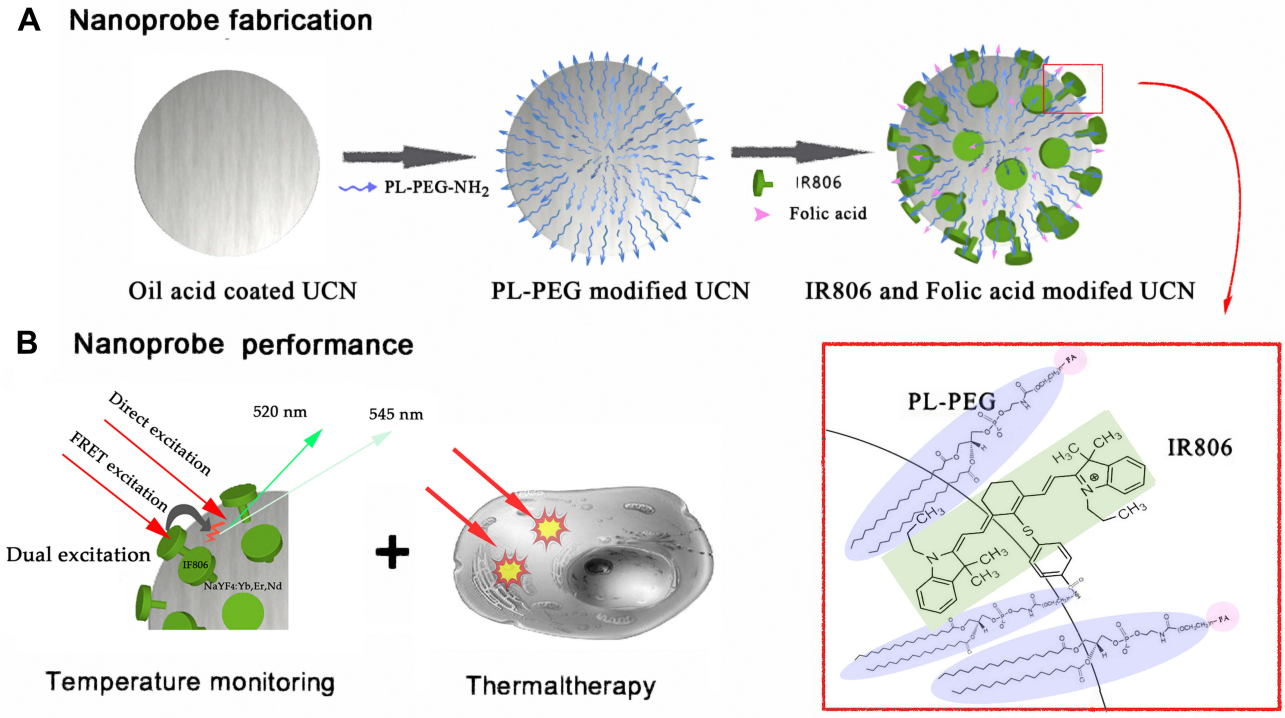

Figure 1 Schematic illustration of the NP fabrication process (**A**) and performance mechanism (**B**).

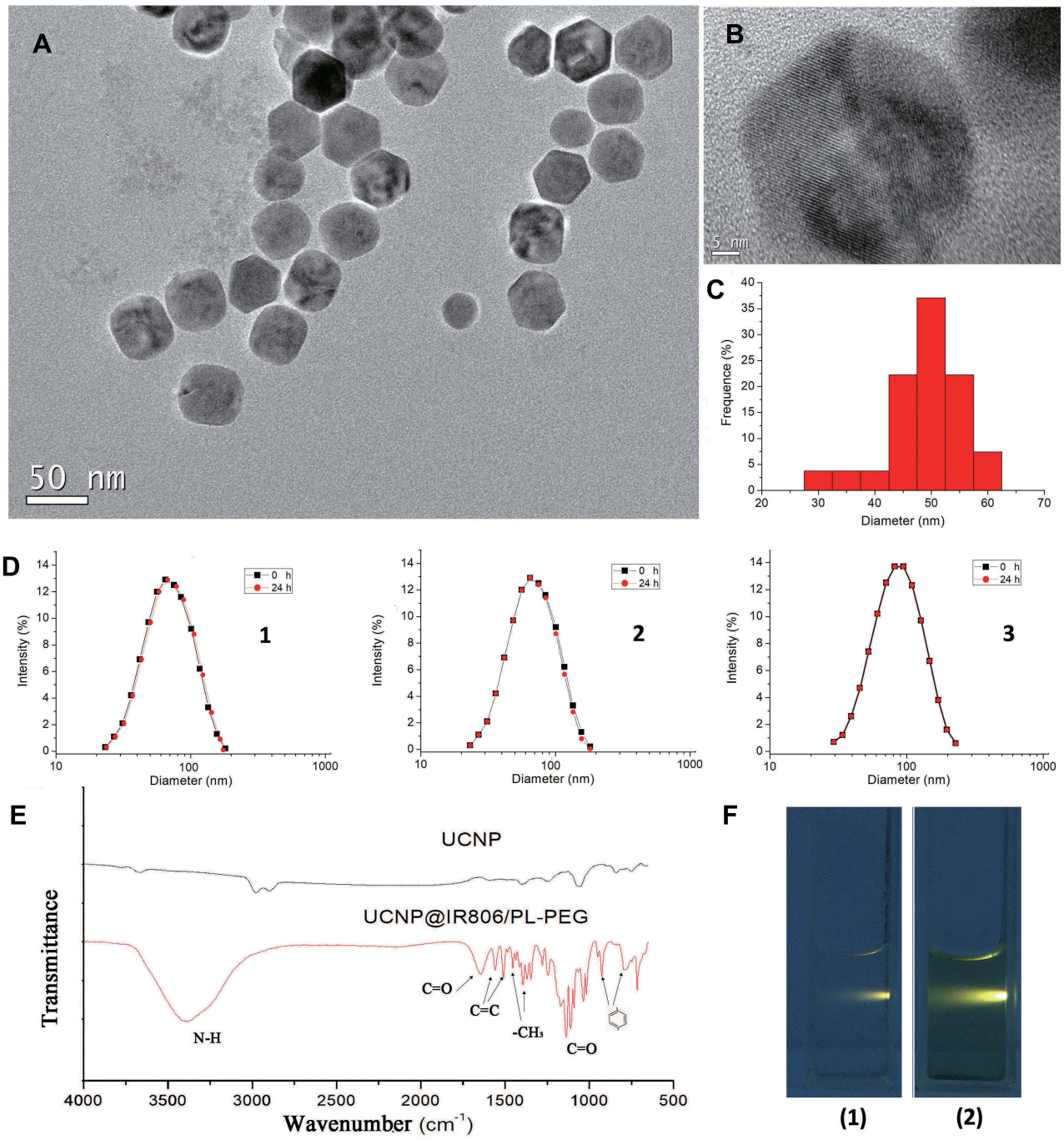

Figure 2 Physical properties of the nanoparticles. (**A**) TEM images of $NaYF_4$:Yb,Er,Nd. (**B**) The ionic lattice geometry of a nanoparticle in a TEM image. (**C**) The statistical size of $NaYF_4$:Yb,Er,Nd measured by TEM. (**D**) DLS 0 and 24 h profile of $NaYF_4$:Yb,Er,Nd@IR-806/PL-PEG-FA in water (1), saline (2) and RPMI 1640 (3) separately. (**E**) FTIR spectra of IR-806 and PL-PEG-capped NaYF4:Yb,Er, Nd. (**F**) Optical images of $NaYF_4$:Yb,Er,Nd@ PL-PEG-FA (1) and $NaYF_4$:Yb,Er,Nd@IR-806/PL-PEG-FA (2) excited by an 808 nm laser.

shown in Figure 2E. Compared to that of the oleylamine-coated UCNs, the IR absorption of IR-806/PL-PEG-coated UCNs displayed an obvious peak change. The spectral patterns of IR-806/PL-PEG and the inorganic NP core confirm the successful molecular modification of the NPs. Figure 2F shows a light emission of UCNs before and after IR-806 coating. The results show that the solution changed from colorless to deep green after coating the UCNs with IR-806 (right image), indicating the successful binding between IR-806 and the nanoparticles. Upon the same light excitation with

an 808 nm laser, a significant enhancement in upconversion luminescence was also observed, suggesting an additional energy transfer pathway.

The absorption and fluorescence spectra of IR-806 are shown in Figure 3A. The absorbance of IR-806 has a peak value at 800 nm, which is near to the excitation light. The concentration of IR-806 can affect its absorption performance, but the peak at 800 nm is more stable than the peak at 720 nm. The ratio of the two peaks was found enhanced when the concentration of IR-806 increases, indicating the possibility of determining the concentration of IR-806 based on the peak ratio (Figure S3). When IR-806 was modified onto the nanoparticles, the detected absorption and fluorescence spectra were similar to the previous spectra, suggesting that IR-806 had been successfully modified onto the particles. With light irradiation, strong absorption by the NPs at 800 nm was observed. The energy was partly transferred to emit fluorescence in the wavelength range from 810 to 1000 nm with a peak at 850 nm (Figure 3B). Upon irradiation with an 808 nm laser, upconversion emission by the NPs also occurred. The visible light emission had three peaks at 520, 545 and 654 nm. Their corresponding energy level transitions are marked in Figure 3C. The green light emission peaks at 520 and 545 nm were specifically detected for a ratio calculation. In addition, the results also indicate that the IR-806 modification can significantly affect the luminescence of the NPs. The results show that the NPs had a strong emission when the modification ratio was at 1:50 (NP: IR-806). However, higher IR-806 concentrations would increase the amount of 808 nm light absorbed by the dye and block the UCNs from absorbing the light. Both the low and high fluorescent ratios could reduce the amount of light emitted.

The luminescence of different nanoparticles with or without Nd^{3+} doping, and with or without IR-806 capping

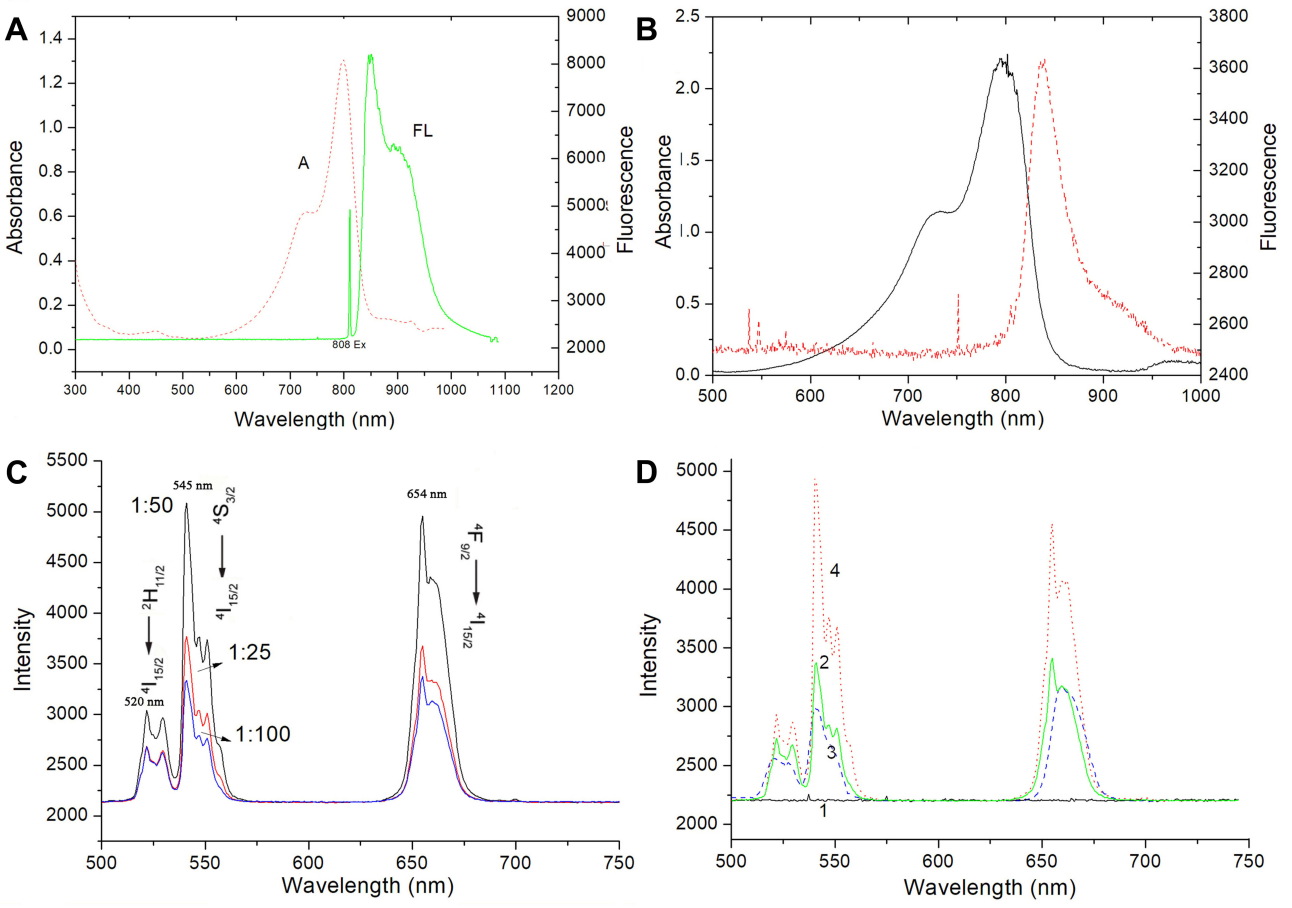

Figure 3 UV–Vis spectra of the upconversion nanoparticles and IR-806. (**A**) The absorbance and fluorescence spectra of IR-806 excited by an 808 nm laser. (**B**) The absorbance and fluorescence spectra of $NaYF_4$:Yb,Er,Nd@IR-806/PL-PEG-FA excited by an 808 nm laser. (**C**) Upconversion emission spectra of the $NaYF_4$:Yb,Er,Nd@PL-PEG-FA nanoparticles as a function of IR-806 concentration. (**D**) The luminescence of different nanoparticles with or without Nd doping and with or without IR-806 capping excited by an 808 nm laser (without Nd ion doping, with (2) and without (1) IR-806 capping; with Nd ion doping, with (4) and without (3) IR-806 capping).

is shown in Figure 3D. The doped Nd ions are the main energy absorption and transfer agent for 808 nm light. Therefore, when NPs without Nd^{3+} doping were excited by an 808 nm laser, no luminescence was observed (Figure 3D1). Interestingly, when these NPs were capped by IR-806, significant luminescence was apparent, indicating that the laser energy had transmitted to the NPs through the FRET process and then to Yb and Er for light emission (Figures 3D2). The FRET process depends on the nanocrystal absorption at 980 nm. To clarify the absorption, the luminescence of the nanocrystal was detected upon excitation with a 980 laser (Figure S4). The result indicates that the nanocrystals could be excited by 980 nm light and that the visible light spectrum was very similar to the spectrum obtained with 808 nm excitation. When irradiating the Nd^{3+}-doped NPs, both those NPs with and without IR-806 as a capping agent exhibited luminescence (Figures 3D4). However, the IR-806-capped NPs exhibited a much brighter luminescence than did those not capped by IR-806 due to the dual-energy transfer mechanism.

As temperature is one of the factors influencing energy level transitions, it can also affect upconversion luminescence. When the temperature increased, the luminescence of the NPs gradually decreased (Figure 4A). However, the influence of different energy states photon emission is different. The decrease in radiative transitions at a high-energy level would be slower than that at a low-energy level when the temperature rises. The relationship between the luminescence ratio of different energy states and

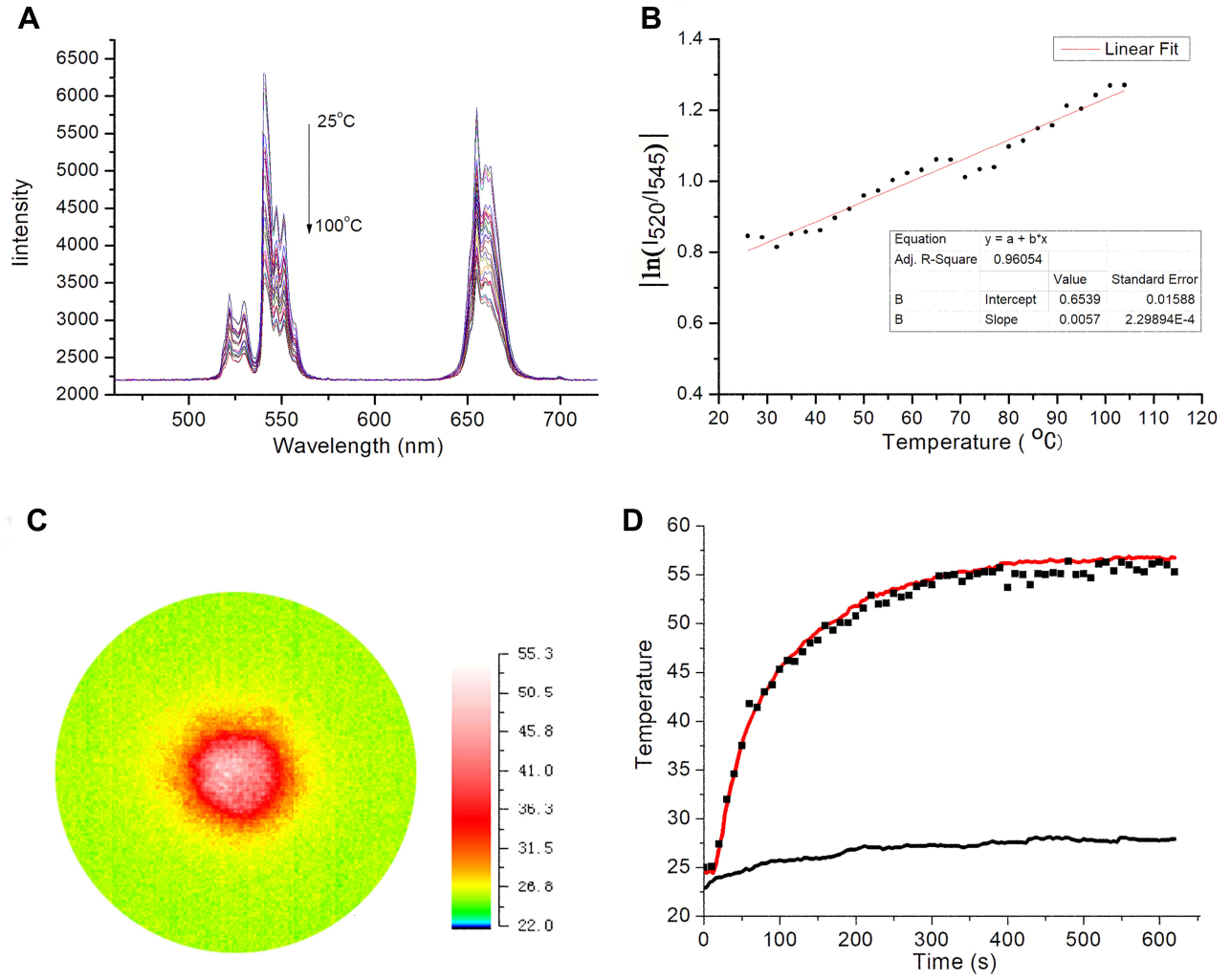

Figure 4 Temperature-sensing properties of the NPs. (**A**) The upconversion emission spectra of NPs excited at 808 nm at different temperatures. (**B**) A plot of I520/I545 versus temperature used to calibrate the thermometric scale of the nanoprobe. I520 and I545 indicate the upconversion emission of the 2H11/2 - 4I15/2 and 4S3/2 - 4I15/2 transitions, respectively. (**C**) Temperature changes of the NPs in a planar dish during irradiation with an 808 nm laser. (**D**) Temperature curves for the NP solution under 808 nm laser irradiation (Solution: 0.2 mg/mL; laser: 0.6 W/cm2; control: water).

temperature can be described with a formula in which the absolute value of the logarithm of the ratio is linearly proportional to the temperature.[13] The detected results and its linear fit are shown in Figure 4B. When irradiated by a laser, the thermal image of NPs in a planar dish was acquired, showing a distinct temperature difference: it was high in the irradiated area and low in other areas (Figure 4C). The rise in temperature of NPs in pure water under laser irradiation as a control is shown in Figure 4D. The temperatures of both solutions were increased. However, the NP solution showed a sharper rise up to 55°C at the later stage than did water under laser irradiation at the same power.

The hyperthermic reaction of upconversion NPs in EMT-6 cells was detected after the cells were incubated by NPs. EMT-6 cells are folic acid receptor overexpressed. The surface of NPs was modified with folic acid molecules as a ligand for the cell targeting. Figure 5A shows that NPs emitted light in cells under laser irradiation, confirming the feasibility of cell endocytosis of the NPs. The dark cytotoxicity of the NPs at different concentrations was studied, showing low toxicity up to 1.6 mg/mL (Figure S5). After hyperthermia treatment, cell apoptosis was observed with Hoechst staining (Figure 5B). Cell death through apoptosis has a great advantage for treatment. Different laser and NP concentration doses were administered to cells. Cell viability was assessed with CCK8 OD450 to determine the photothermal effects. Figure 5C and D indicate that the cells could be killed after the hyperthermic reaction but the cell viabilities changed with different doses of irradiation time and NP concentration. The results showed the controllable and effective thermal effects of the NPs, suggesting their potential for thermal therapy applications. Too low and too high doses were not suitable for effective treatment. Therefore, a preferred treatment dose (0.5 mg/mL, laser: 0.6 W/cm^2) was selected and used for cells in this study.

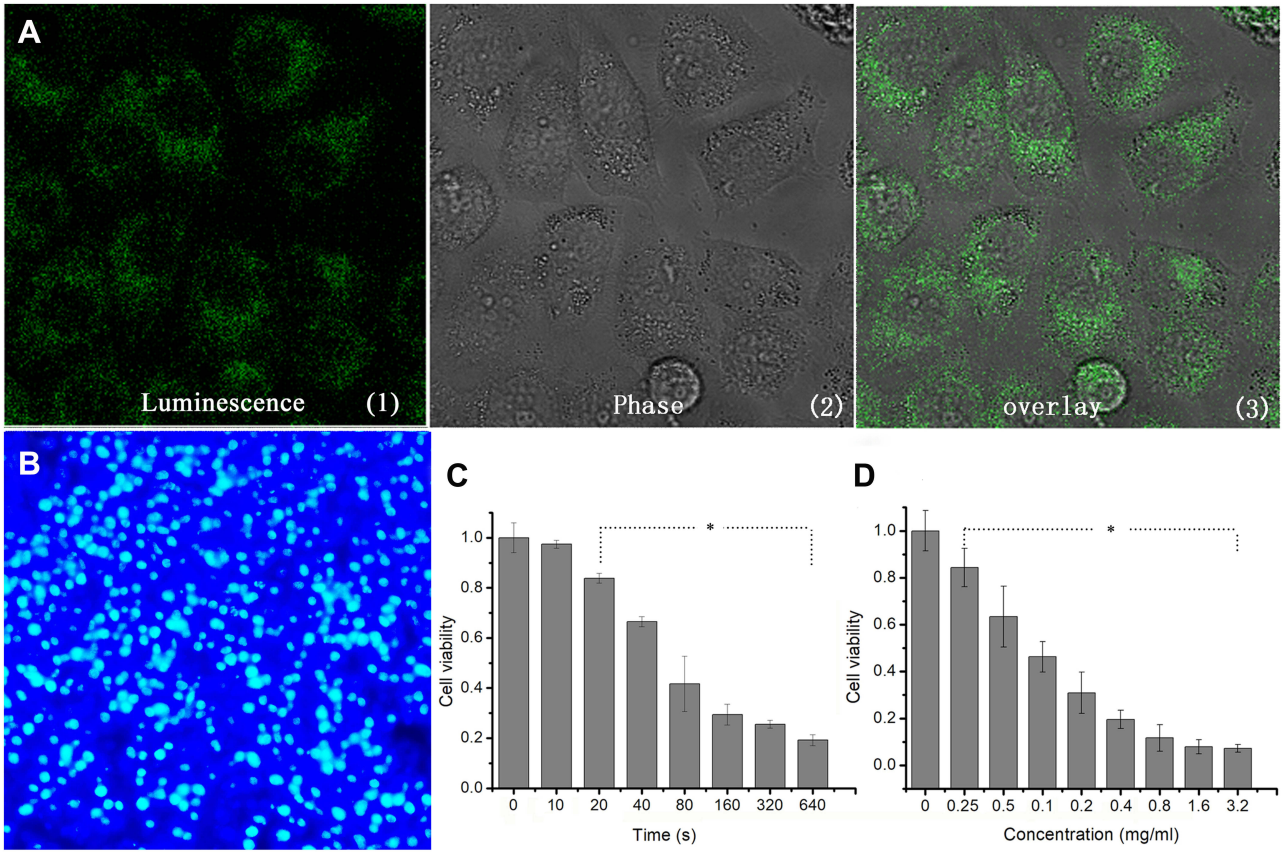

Figure 5 Luminescence and hyperthermic reactions of upconversion NPs on cells. (**A**) Luminescence and light images and their overlay of upconversion NPs in cells. (**B**) Imaging of Hoechst staining to confirm the hyperthermic effect of upconversion NPs in cells (nanoprobe: 0.5 mg/mL, laser: 0.6 W/cm^2). (**C**) Cell viability after hyperthermia treatment with different laser irradiation times (time: 0–640 s, concentration: 0.5 mg/mL, laser: 0.6 W/cm^2). (**D**) Cell viability after hyperthermia treatment with different nanoprobe concentrations (concentration: 0.025–3.2 mg/mL, laser: 0.6 W/cm^2, time: 500 s). For all experiments, data represent the mean ± S.D. of four independent experiments. Asterisk means a Student's *t*-test to compare with the left Control groups, $P < 0.05$ (n=4).

When temperature is precisely controlled during thermal treatment, the final outcome will be enhanced greatly, and side effects will be minimized. The results of NPs in cells suggested the possibility of their use for tumor treatment with simultaneous thermal reactions and temperature monitoring. Based on the cell data, in vivo effects on mice were then studied.

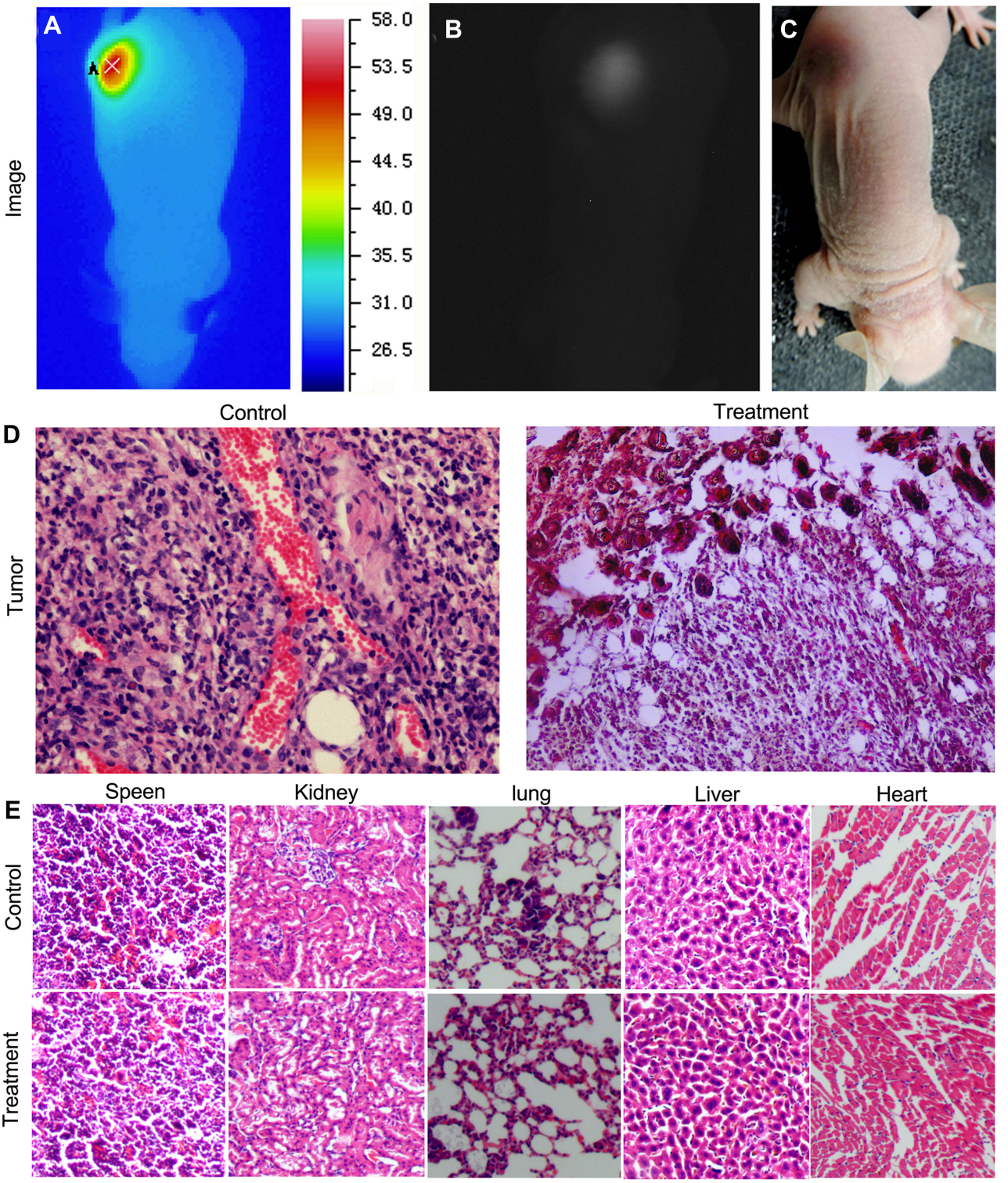

Figure 6 Hyperthermic reaction of upconversion NPs on mice. (**A**) and (**B**) Thermal imaging and upconversion luminescence imaging of a mouse 12 h after NPs were injected intravenously (nanoprobe injection: 100 μL of NPs with a concentration at 10 mg/mL, laser fluence rate of 0.8 W/cm^2). (**C**) Visible light imaging after hyperthermal treatment of the mouse. (**D**) H&E histologic sections of the tumor after hyperthermal treatment and of the control. (**E**) H&E histologic section of the major organs after hyperthermal treatment and that of the control.

Tumor-bearing mice were subjected to thermal treatment 6 hrs after NPs were injected intravenously. Temperature and upconversion luminescence were imaged with a thermal machine and a CCD camera, respectively, as the mouse tumor was irradiated with a laser (Figure 6A and B). The results showed temperature increase and significant upconversion luminescence in the tumor area, suggesting that the NPs had accumulated at the tumor site and induced strong light energy absorption. The highest temperature reached up to 51.2°C at that treatment dose. At 12 hrs after the thermal therapy, visible light imaging showed that the skin in the tumor area exhibited a color change (Figure 6C). After the mouse was then sacrificed to obtain the bulk tumor, a large number of apoptotic cells were in the H&E section of tumor compared to that of the control, indicating that the efficient hyperthermic effects were achieved by using the near-infrared NPs (Figure 6D). In addition, there was no obvious difference of the organ H&E sections between the treated mouse and the control mouse (Figure 6E). The results indicate that the toxicity of the NPs was low enough.

The results in vitro and in vivo exhibited a virtuous effect for tumor treatment; however, the long-term therapy outcome still should be seriously mentioned. It is known that tumor can be recurrence after an inadequate treatment. The long-term therapeutic outcome is often verified by measuring the volume of tumors over several weeks.[32,33] Indeed, due to the rich blood vessels and diverse components, the living tissue of tumor has complex thermal distribution during photothermal therapy, leading to inadequate treatment and uncertain therapeutic effect. Therefore, it is necessary for photothermal therapy to accurately monitor the temperature of each part of tumor tissue and control the local dose of light for effective treatment. Only in this way can the application of the NPs kill tumor cells neatly and reduce the damage to normal tissues, realizing a long-term curative effect. Accordingly, in the next study, we will focus on the thermal therapy in combination with the spatially resolved real-time temperature detection to realize adequate tumor treatment for fully revealing the long-term effect of the NP-based thermal therapy.

Conclusions

In this study, IR-806 dye was modified on the upconversion nanocrystal surface to transfer light energy for inducing thermal effect and upconversion luminescence. The modification of IR-806 as a molecular antenna showed distinct advantages: first, the minimal absorption by water to the excitation light of IR-806 avoided energy transmission lose and enhanced tissue penetration; Second, IR-806 had stronger absorption of near-infrared light than did the Nd ions of the nanoparticle and thus enhanced the energy transfer during light irradiation; Third, two approaches for energy transfer to the Yb ions of the NPs, include a FRET process energy transfer from IR-806 and a migration process energy transfer from Ed ions, co-enhanced the NP luminescence. Based on the molecular antenna modification and irradiated with a monochromatic light, the synthesized NPs exhibited high near-infrared light absorption and brighter upconversion luminescence, and realized effective thermal treatment and simultaneous temperature monitoring. The NPs are promising to be used for light ratio temperature detection and effective thermal therapy of tumors, as well as biological imaging.

Statistical Analysis

Data were presented as mean ± SD. The in vitro results were tested with the Student's *T*-test for any statistical difference. A value of $P < 0.05$ was considered statistically significant.

Abbreviations

PTT, photothermal therapy; UCNs, upconversion nanocrystals; NPs, nanoprobes; FRET, fluorescence resonance energy transfer.

Acknowledgments

This research is supported by the National Natural Science Foundation of China (51775221, 31870952), Science Technology Program Guangzhou (201607010371), the Natural Science Foundation of Jiangsu Provincial Department of Education (17KJB530001), and Natural Science Foundation of Jiangsu Province of China (BK20181480).

Disclosure

The authors report no conflicts of interest in this work.

References

1. Kim HS, Lee DY. Near-infrared-responsive cancer photothermal and photodynamic therapy using gold nanoparticles. *Polymers*. 2018;10(9):961. doi:10.3390/polym10090961
2. Wu Q, Xia N, Long D, et al. Dual-functional supernanoparticles with microwave dynamic therapy and microwave thermal therapy. *Nano Lett*. 2019;19(8):5277–5286. doi:10.1021/acs.nanolett.9b01735
3. Hea-Jong Chung H-KL, Kwon KB, Kim H-J. Seong-Tshool Hong Transferrin as a thermosensitizer in radiofrequency hyperthermia for cancer treatment. *Sci Rep-Uk*. 2018;8(1):13505. doi:10.1038/s41598-018-31232-9
4. Nam J, Son S, Ochyl LJ, Rui K, Schwendeman A, Moon JJ. Chemo-photothermal therapy combination elicits anti-tumor immunity against advanced metastatic cancer. *Nat Commun*. 2018;9(1):1074. doi:10.1038/s41467-018-03473-9

5. Alves CG, de Melo-diogo D, Lima-Sousa R, Costa EC, Correia IJ. Hyaluronic acid functionalized nanoparticles loaded with IR780 and DOX for cancer chemo-photothermal therapy. *Eur J Pharm Biopharm*. 2019;137:86–94. doi:10.1016/j.ejpb.2019.02.016
6. Chen Q, Chen J, He M, et al. Novel small molecular dye-loaded lipid nanoparticles with efficient near-infrared-II absorption for photoacoustic imaging and photothermal therapy of hepatocellular carcinoma. *Biomater Sci*. 2019;7(8):3165–3177. doi:10.1039/C9BM00528E
7. Feng Z, Yu X, Jiang M, et al. Excretable IR-820 for in vivo NIR-II fluorescence cerebrovascular imaging and photothermal therapy of subcutaneous tumor. *Theranostics*. 2019;9(19):5706–5719. doi:10.7150/thno.31332
8. Gao G, Jiang YW, Sun W, et al. Molecular targeting-mediated mild-temperature photothermal therapy with a smart albumin-based nanodrug. *Small*. 2019;15(33):e1900501. doi:10.1002/smll.201900501
9. Cui L, Xiong C, Zhou M, Shi S, Chow DS, Li C. Integrin alphavbeta3-targeted [(64)Cu]CuS nanoparticles for PET/CT imaging and photothermal ablation therapy. *Bioconjug Chem*. 2018;29(12):4062–4071. doi:10.1021/acs.bioconjchem.8b00690
10. Sun T, Han J, Liu S, Wang X, Wang ZY, Xie Z. Tailor-made semiconducting polymers for second near-infrared photothermal therapy of orthotopic liver cancer. *ACS Nano*. 2019;13(6):7345–7354. doi:10.1021/acsnano.9b03910
11. Zhang M, Wang W, Cui Y, Zhou N, Shen J. Near-infrared light-mediated photodynamic/photothermal therapy nanoplatform by the assembly of Fe3O4 carbon dots with graphitic black phosphorus quantum dots. *Int J Nanomedicine*. 2018;13:2803–2819. doi:10.2147/IJN.S156434
12. de Witte P, de Witt CA, van de Minkelis JL, et al. Inflammatory response and optimalisation of perioperative fluid administration during hyperthermic intraoperative intraperitoneal chemotherapy surgery. *J Gastrointest Oncol*. 2019;10(2):244–253. doi:10.21037/jgo
13. Zhu X, Feng W, Chang J, et al. Temperature-feedback upconversion nanocomposite for accurate photothermal therapy at facile temperature. *Nat Commun*. 2016;7:10437. doi:10.1038/ncomms10437
14. Ribeiro KL, Frias IAM, Franco OL, et al. Clavanin A-bioconjugated Fe3O4/Silane core-shell nanoparticles for thermal ablation of bacterial biofilms. *Colloids Surf B Biointerfaces*. 2018;169:72–81. doi:10.1016/j.colsurfb.2018.04.055
15. Lo WC, Uribe-Patarroyo N, Nam AS, Villiger M, Vakoc BJ, Bouma BE. Laser thermal therapy monitoring using complex differential variance in optical coherence tomography. *J Biophotonics*. 2017;10(1):84–91. doi:10.1002/jbio.201600072
16. Hu X, Li Y, Liu T, Zhang G, Liu S. Intracellular cascade FRET for temperature imaging of living cells with polymeric ratiometric fluorescent thermometers. *ACS Appl Mater Interfaces*. 2015;7(28):15551–15560. doi:10.1021/acsami.5b04025
17. Del Rosal B, Carrasco E, Ren F, et al. Infrared-emitting QDs for thermal therapy with real-time subcutaneous temperature feedback. *Adv Funct Mater*. 2016;26(33):6060–6068. doi:10.1002/adfm.201601953
18. Hou B, Jia M, Li P, Liu G, Sun Z, Fu Z. Multifunctional optical thermometry based on the rare-earth-ions-doped up-/down-conversion Ba2TiGe2O8: ln(Ln = Eu(3+)/Er(3+)/Ho(3+)/Yb(3+)) phosphors. *Inorg Chem*. 2019;58(12):7939–7946. doi:10.1021/acs.inorgchem.9b00646
19. Liu H, Zuo C, Liu Y, et al. Optical thermometry through infrared excited green upconversion of KLa (MoO4) 2: yb3+/Er3+ phosphor. *J Lumin*. 2019;207:93–97. doi:10.1016/j.jlumin.2018.11.010
20. Fang W, Wei Y. Upconversion nanoparticle as a theranostic agent for tumor imaging and therapy. *J Innov Opt Health Sci*. 2016;9(4):1630006. doi:10.1142/S1793545816300068
21. Li K, Hong E, Wang B, et al. Advances in the application of upconversion nanoparticles for detecting and treating cancers. *Photodiagnosis Photodyn Ther*. 2019;25:177–192.
22. Zhu X, Wang H, Zheng L, et al. Upconversion nanoparticle-mediated photodynamic therapy induces THP-1 macrophage apoptosis via ROS bursts and activation of the mitochondrial caspase pathway. *Int J Nanomedicine*. 2015;10:3719–3736. doi:10.2147/IJN.S82162
23. Shi J, Zhao Z, Liu Z, Wu R, Wang Y. Ultralow-intensity NIR light triggered on-demand drug release by employing highly emissive UCNP and photocleavable linker with low bond dissociation energy. *Int J Nanomedicine*. 2019;14:4017–4028. doi:10.2147/IJN.S201982
24. Wiesholler LM, Frenzel F, Grauel B, Würth C, Hirsch T. Yb,Nd,Er-doped upconversion nanoparticles: 980 nm versus 808 nm excitation. *Nanoscale*. 2019;11(28):13440–13449. doi:10.1039/C9NR03127H
25. Wang D, Xue B, Kong X, et al. 808 nm driven Nd3+-sensitized upconversion nanostructures for photodynamic therapy and simultaneous fluorescence imaging. *Nanoscale*. 2015;7(1):190–197. doi:10.1039/C4NR04953E
26. Wei Y, Chen Q, Wu B, Xing D. Excitation-selectable nanoprobe for tumor fluorescence imaging and near-infrared thermal therapy. *J Biomed Nanotechnol*. 2016;12(1):91–102. doi:10.1166/jbn.2016.2198
27. Zou W, Visser C, Maduro JA, Pshenichnikov MS, Hummelen JC. Broadband dye-sensitized upconversion of near-infrared light. *Nat Photonics*. 2012;6(8):560–564. doi:10.1038/nphoton.2012.158
28. Huang X. Broadband dye-sensitized upconversion: a promising new platform for future solar upconverter design. *J Alloys Compd*. 2017;690:356–359. doi:10.1016/j.jallcom.2016.08.142
29. Chai X, Li J, Wang X, Li Y, Yao X. Upconversion luminescence and temperature-sensing properties of Ho 3+/Yb 3+-codoped ZnWO 4 phosphors based on fluorescence intensity ratios. *RSC Adv*. 2017;7(64):40046–40052. doi:10.1039/C7RA05846B
30. Wu C, Wang S, Zhao J, et al. Biodegradable Fe (III)@ WS2-PVP Nanocapsules for redox reaction and TME-enhanced nanocatalytic, photothermal, and chemotherapy. *Adv Funct Mater*. 2019;29(26):1901722. doi:10.1002/adfm.v29.26
31. Wei Y, Quan L, Zhou C, Zhan Q. Factors relating to the biodistribution & clearance of nanoparticles & their effects on in vivo application. *Nanomedicine (Lond)*. 2018;13(12):1495–1512. doi:10.2217/nnm-2018-0040
32. Zheng Y, Wang W, Zhao J, et al. Preparation of injectable temperature-sensitive chitosan-based hydrogel for combined hyperthermia and chemotherapy of colon cancer. *Carbohydr Polym*. 2019;222:115039. doi:10.1016/j.carbpol.2019.115039
33. Liu Y, Xi Y, Zhao J, et al. Preparation of therapeutic-laden konjac hydrogel for tumor combination therapy. *Chem Eng J*. 2019;375:122048. doi:10.1016/j.cej.2019.122048